


RESEARCH ARTICLE | JULY 22 2021

Rock and roll: Incipient aeolian entrainment of coarse particles

Zhao Xiao-Hu (赵小虎); Manousos Valyrakis  ; Li Zhen Shan (李振山)



Physics of Fluids 33, 075117 (2021)

<https://doi.org/10.1063/5.0047604>



View
Online



Export
Citation

CrossMark

Articles You May Be Interested In

Entrainment of coarse grains using a discrete particle model

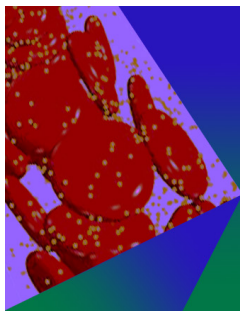
AIP Conference Proceedings (October 2014)

Effects of Wire Resonance on Aeolian Tones

J Acoust Soc Am (July 2005)

Aeolian Tones

J Acoust Soc Am (June 2005)



Physics of Fluids

Special Topic: Flow and Forensics

Submit Today!



Rock and roll: Incipient aeolian entrainment of coarse particles



Cite as: Phys. Fluids **33**, 075117 (2021); doi: [10.1063/5.0047604](https://doi.org/10.1063/5.0047604)

Submitted: 15 February 2021 · Accepted: 7 July 2021 ·

Published Online: 22 July 2021



View Online



Export Citation



CrossMark

Zhao Xiao-Hu (赵小虎),¹ Manousos Valyrakis,^{2,3,a)}  and Li Zhen Shan (李振山)^{4,5}

AFFILIATIONS

¹Division of Environmental Management and Policy, School of Environment, Tsinghua University, 100084 Beijing, China

²School of Engineering, University of Glasgow, G12 8LT Glasgow, United Kingdom

³Water Engineering Laboratory, College of Science and Engineering, University of Glasgow, G12 8LT Glasgow, United Kingdom

⁴College of Environmental Science and Engineering, Peking University, 100871 Beijing, China

⁵The Key Laboratory of Water and Sediment Sciences, Ministry of Education, Peking University, 100871 Beijing, China

^{a)}Author to whom correspondence should be addressed: Manousos.Valyrakis@glasgow.ac.uk

ABSTRACT

Aeolian transport of coarse grains is an important topic, finding applications in nature (for infrastructure exposed to wind scour) as well as industry (e.g., considering pneumatic transport). Incipient particle entrainment due to turbulent winds refers to the wind conditions where aeolian transport initiates, and as such, it is at the core of such studies. The research presented herein focuses on identifying and quantifying the dynamical processes responsible for coarse particle entrainment. Specifically designed wind tunnel experiments are conducted for a range of wind conditions near the aeolian transport thresholds. A high-resolution laser distance sensor is employed to provide information for the displacement of an exposed particle ranging from small simple rocking motions to complete entrainments (rolling). Measurements of the exposed particle's angular displacements are acquired, which allow the probabilistic study of incipient motion. The variation of statistical parameters, such as the frequency of entrainments, duration of dislodgements, magnitude of displacements, and time between displacements, is studied for a range of increasing airflow rates. The main findings from these experiments suggest that rocking can be observed only up to a limit angular displacement (equal to 0.41π for the conditions tested herein), which defines the position beyond which the resistance force can be overcome by just the mean aerodynamic forcing. Following this experimental framework to establish aeolian thresholds for a wider range of environments may be useful for the identification of the wind conditions under which aeolian transport may start occurring.

© 2021 Author(s). All article content, except where otherwise noted, is licensed under a Creative Commons Attribution (CC BY) license (<http://creativecommons.org/licenses/by/4.0/>). <https://doi.org/10.1063/5.0047604>

I. INTRODUCTION

Incipient aeolian grain entrainment is an important challenge finding application for a wide range of topics spanning aeolian sediment entrainment (Bagnold, 1941; Pähtz *et al.*, 2020), and aeolian creep transport (Wang *et al.*, 2020; Zhang *et al.*, 2021a), to bedform transport in the form of sand waves and ripples (Sherman *et al.*, 2018; Liu *et al.*, 2020). These processes are also important for industrial applications such as pneumatic transport (Molerus and Burschka, 1995; Molerus, 1996). Advances in the understanding of these transport processes are slow due to the difficulties in assessing and characterizing the interactions of particles and turbulent airflows. The rich dynamics exhibited by grains transported by aerodynamic forces has been studied both experimentally and numerically. For example, Zhang *et al.* (2020) used wind tunnel experiments to physically model the aeolian entrainment of grains flux, to derive scaling laws between the rate of grain entrainment and average surface shear stresses, and to

model these with a predictive model that accounts for turbulence. Relevant numerical investigations account for the interactions between particles for coarse and cohesive (including snow) entrainment (Pähtz and Duran, 2020; Jia and Wang, 2021). In the presence of a near threshold wind flow field, the entrained particle is observed to first start rock within its resting pocket—a process that has also been described as “vibration” or “wobbling” (Lyles, 1977; Greeley and Marshall, 1985; Skidmore, 1986; Nickling, 1988; Anderson *et al.*, 1991; Shi *et al.*, 2004). As the flow increases further, rolling and saltation may follow up leading to its complete entrainment and subsequent transport downwind. Such observations render valuable the further study of incomplete and full entrainment events, termed here as rocking and rolling, respectively. Inspired by the advances in the literature of fluvial grain entrainment showcasing the importance of hydrodynamic impulses (e.g., Celik *et al.*, 2010; Dwivedi *et al.*, 2011; Diplas *et al.*, 2008) or energetic flow events (Lee *et al.*, 2012; Valyrakis *et al.*,

2013), and the similarities between the aeolian and fluvial grain transport processes (Giménez-Curto and Corniero, 2009; Pähtz and Duran, 2020; Pähtz *et al.*, 2020), this study aims to characterize and stochastically describe the occurrence of intermittent and distinct particle motions induced by sufficiently energetic aerodynamic turbulence. Expansion of the impulse or work criterion into the field of aeolian transport may benefit from detailed measurements of the threshold elevation parameter during aeolian induced transport.

Past research used visual methods to obtain grain trajectories during transport (e.g., Bisal and Nielsen, 1962; Williams *et al.*, 1994). Herein, the focus is on designing a series of aeolian entrainment wind tunnel experiments to assess the minute motions before and during incipient grain entrainment. To this goal, the movement of a target particle (medium gravel size), resting on an aerodynamically rough flat surface, is conducted using a high-resolution laser distance detector. An aerodynamically rough bed surface comprises of bed surface particles of the same size as the target particle that is fully exposed to the wind aerodynamic drag and, thus, is expected to be the first to be entrained. The bed surface is flat and horizontal to remove any effects of bed forms creating macroscale wind flow structures. The bed surface particles form a well packed orthogonal arrangement. In this fashion, aerodynamic roughness scales with the size of the bed surface particles and particle entrainment is mainly controlled by the flow structures impinging at the bed surface, rather than any other unsteady or macroscale flow features. Particle motion characteristics (including frequency of motions, their duration, magnitude, and time between entrainments), as well as the transition from rocking to rolling motions, are specifically studied and assessed considering their modeled distribution functions.

II. EXPERIMENTAL PROTOCOL AND CRITERIA FOR PARTICLE ROCKING

A. Experimental procedure

The experiments are conducted in an environmental wind tunnel in Peking University. The suction-type, non-circulating wind tunnel has a length of 50 m, a 30 m long usable section, and a width of 3 m. The cross-sectional area of the test section is $3.4 \times 2.4 \text{ m}^2$ (Fig. 1). The test section is 30 cm distant from the wind tunnel walls, to allow transporting and positioning the test section when setting up the experiment. The effect of slightly reduced bed roughness near the walls is compensated by the relative effect of increased shear stresses due to the wind tunnel side walls. The free-stream mean wind speed (U) within the wind tunnel is controlled and can range from 0.5 to 20 m/s. The large dimensions of the wind tunnel used herein allow for a fairer representation of the flow structures responsible for aeolian transport compared to smaller wind tunnels (Pähtz *et al.*, 2018).

The experimental test section that comprises of a layer of a 40 mm table tennis plastic spheres is sized to be a 4 m long and a 2.4 m wide and starts a 22.6 m downwind from the entrance of the wind tunnel, ensuring that the turbulent boundary layer is fully developed (Fig. 1). This is validated by taking velocity profiles at consecutive locations every 0.5 m downwind and along the centerline of the wind tunnel, observing that the boundary layer has been fully developed and remains practically unchanged. The test section, is sufficiently long for the turbulent boundary layer flow to fully develop. The test particle is exposed to, at the centerline of the wind tunnel, resting on top or an aerodynamically roughened bed surface. The boundary layer

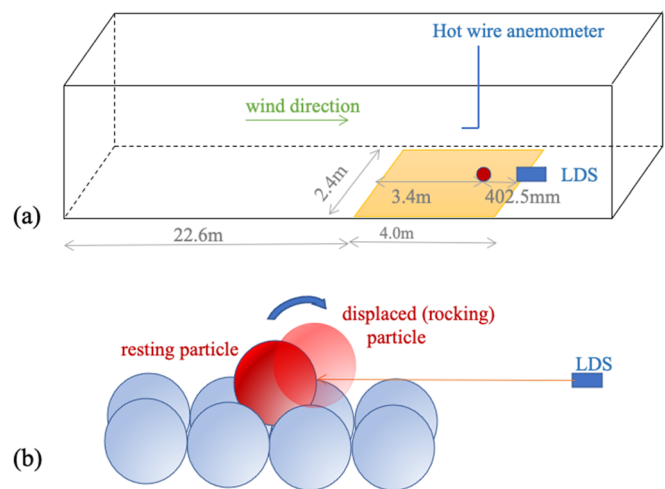


FIG. 1. Sketch of the experimental setup (not drawn to scale): (a) wind tunnel and test section with the relevant placement of the exposed particle and anemometry (hot-wire) and distance (LDS) tracking instrumentation (also showing relevant dimensions and the wind direction), and (b) side perspective view of the target exposed particle resting on a pocket of same size spherical particles forming a tightly packed orthogonal arrangement (also showing the displaced particle position). The resting downstream particle at a distance of 402.5 mm is located the LDS, used for capturing particle rockings and full displacements.

conditions above the bed surface are shown in Fig. 2, where the average wind speed profile is observed to follow the typical logarithmic law, and maximum turbulence is measured to be around 20% near the surface. The local flow measurements are taken in a way to optimally capture the logarithmic rate of change in the flow from the bed surface, leading to a greater spatial resolution near the solid rough boundary (every 1 mm) and a lower density of measurements above 500 mm (e.g., only three measurement points per 100 mm from 500 to 600 mm). Hot-wire anemometry is used for taking local (point) wind speed records at a frequency of data acquisition of 1000 Hz, for a duration of at least 1 min. By means of obtaining these local records for each distinct location across the height of the profile, and subsequently averaging, the mean wind speed profile shown in Fig. 2(b) is obtained.

The test sphere weighs 2.7 g and is identical with those constituting the bed surface. It is exposed fully in the quadrate pocket positioned at the centerline of the bed and 3.4 m downwind from the leading edge (Fig. 1). The use of lightweight spheres (with solid density about 67 times the air density) for studying incipient aeolian entrainment is a novel approach, which allows conducting wind tunnels experiments at lower than usual air flow speeds (due to the lower grain resistance that is proportional to the particle's weight). If natural sediments having a similar size of the test sphere are employed in these experiments, a high-speed tunnel of airflow up to 100 m/s would be required (Batt and Peabody, 1999). Furthermore, even though the testing particle is lighter than natural gravels, it is much heavier than air. This implies that the dynamical process of incipient motion for the experiments described herein is still governed by the balance of aerodynamic force driving entrainment and resisting forces due to its weight, similar to aeolian transport in nature. Likewise, in incipient entrainment studies due to turbulent water flows, similar dynamic

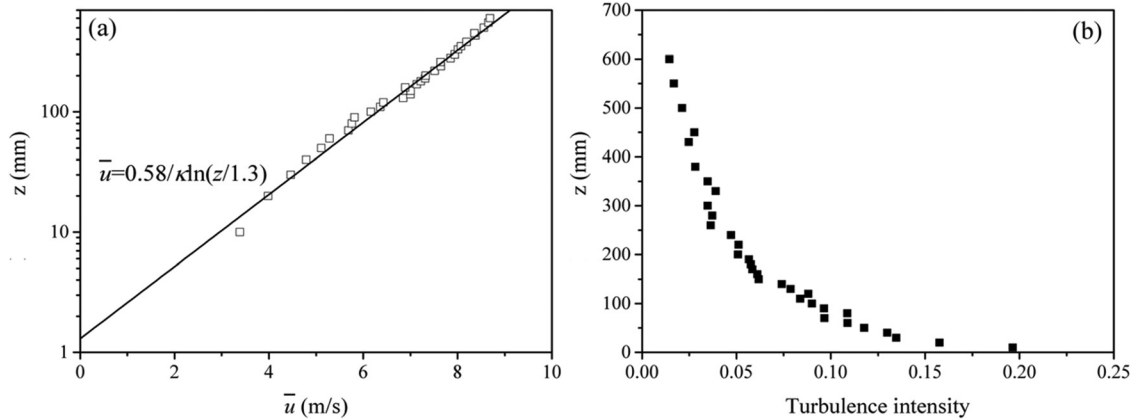


FIG. 2. (a) Mean wind velocity and (b) turbulence intensity profiles. The theoretical bed surface (zero-height) reference level is defined to be at the tops of the well packed spheres comprising the flat bed surface of the test section. The von Karman constant κ is equal to 0.4.

scaling relationships can be used (based on Froude or Reynolds numbers).

The displacement of the test sphere is recorded by a high-resolution (accuracy greater than 0.1 mm) laser distance sensor (LDS, made by Leuze Electronics, Germany). The LDS is fixed at 402.5 mm downwind from the front of the sphere (as shown in Fig. 1), to minimize any disturbances to the local airflow field. Similar non-intrusive setups for monitoring the probability of bed material transport have been also used for fluvial environments (Diplas *et al.*, 2010a, 2010b). The 655 nm red laser light emitted by LDS targeted the center of the test sphere. Calibration of the setup showed that the measured displacement of the target particle is a linear function of the signal intensity of the sensor. Such a setup allows us to obtain the angular displacement of the sphere from the output of LDS based on pocket geometry. The 1000 Hz frequency raw signal from the LDS is smoothed using a 50-points adjacent-averaging method. The size of the moving average window is empirically found (after a trial of different sizes ranging from 10 to 100 data points) to be 50 points, which sufficiently allows both for removing high-frequency noise inherent in the signal and, at the same time, clearly observing the start of particle entrainment. The resultant sampling frequency of the output signal for tracking particle displacement is 20 Hz. Other methods could likewise be used for removing the noise, such as spectral averaging and bandpass filtering (i.e., Zhang *et al.*, 2021b).

The time-averaged freestream wind speed (U) for experiments is set to slightly vary only from 7.5 to 8.2 m/s. The speed range is experimentally defined after trying a wider range of wind speeds, over which the test sphere’s motion can be observed to occur. Specifically, it is seen that there is no movement for $U < 7.5$ m/s and rapid ejection from the sphere’s resting pocket for $U > 8.2$ m/s. Care is taken so that the rate of change in wind speed while approaching the incipient motion conditions is very slow to avoid any additional unsteady aerodynamic forcing on the particle. Flow conditions changing at a rate of about 0.1 m/s per 20 min allow for the flow field to be considered steady for all practical purposes. For the range of airflows tested above, the sampling durations, which are limited by the time to take the target particle to move out of the measuring range of the laser distance sensor, varied from a few seconds to several minutes. The longest

observation duration is limited to 900 s for a flow condition in which the target particle did not escape from the resting pocket. Following the presented methodology, twenty-four runs (E1–E24) are conducted representing different (increasing velocity) but near incipient motion flow conditions summarized in Table 1. During the first four runs (7.5–7.8 m/s), the particle would only perform minute displacement’s rocking events. During the rest of the runs (7.9–8.2 m/s), both rocking and complete rolling of the test particle are observed. Even though the time-averaged free stream speed U is about the same for all these experiments, the rate of occurrence of rocking (f_{rc}) and rolling (f_{rl}) is observed to change more than an order of magnitude. This observation signifies that a mean streamflow criterion is not ideal for appreciating the range of dynamics during sphere’s entrainments.

B. Definition of rocking parameters

A rocking event generally involves two phases as shown in Fig. 3: (a) an downwind ascending phase where the sphere moves from its resting position to the highest, defined by the peak of the saddle formed by the two downwind bed surface particles, and (b) an upwind descending phase where the sphere returns from the peak to the resting position. The rocking parameters, which may be relevant to characterize turbulence-particle dynamical interactions, include the angular amplitude ($\Delta\theta_m$), ascending duration (t_a), and interval time (t_i) between two consecutive rocking events.

III. RESULTS AND DISCUSSION

A. Variation of displacement events

A total of 587 displacement events are detected in experiments, from which two types of movement scenarios are identified, including

TABLE I. Summary of the mean wind and particle motion characteristics for the conducted incipient entrainment experiments.

	U (m/s)	f_{rc} (count/s)	f_{rl} (count/s)
E1–E4	7.5–7.8	0.005 56–0.0344	0
E5–E24	7.9–8.2	0.0689–0.299	0.001 43–0.194

Downloaded from http://pubs.aip.org/aip/pof/article-pdf/doi/10.1063/5.0047604/13831581/075117_1_online.pdf

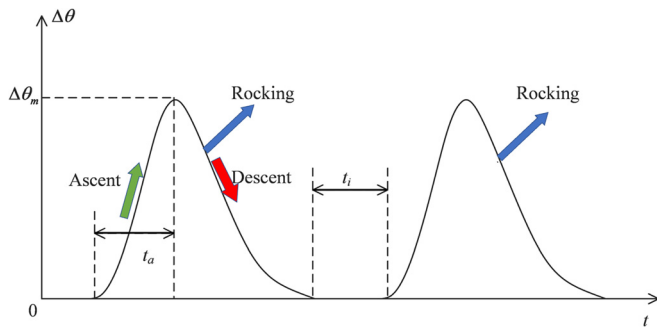


FIG. 3. Sketch of the exposed particle rocking parameters including the amplitude of angular displacement ($\Delta\theta_m$), duration of the particle's ascending motion (t_a), and interval time between rocking events (t_i).

568 rocking (incomplete entrainment events) and 19 incipient rolling (full entrainment) events. Figure 4 shows a range of representative scenarios for both incomplete (cases a–f) and full (cases g–h) incipient entrainment events. Interpreting these figures, it is of interest to consider the transfer of flow momentum toward particle entrainment.

Similar to the impulse criterium for entrainment (proposed by Diplas *et al.*, 2008 and Valyrakis *et al.*, 2010b), the ascent phases can be considered to be the result of a locally advected aerodynamic flow structure imparting a force in excess of the critical resisting force, for a sufficient amount of time, resulting in a positive transfer of momentum. The full rolling motion is achieved when either the combination of the total force or the duration of its application results in a positive aerodynamic impulse that is equal to or greater than the critical impulse.

Depending on the number of entrainment and corresponding rebounding events, represented as peaks and troughs in the displacement history of the test sphere [see Figs. 4(a)–4(f)], the test sphere's rocking motion can be classified into two broad categories: (a) weak or nearly instantaneous rocking events, characterized by a single-peak [Fig. 4(a)], and (b) multiple-peaked rocking events [Figs. 4(b)–4(f)]. The single-peak rocking events typically consist of individual ascent–descent cycles [Fig. 4(a)]. Occasionally, the single-peak rocking events include a minor peak in the upwind direction [Fig. 4(b)] indicative of small rebounding motions due to the impact of the test particle with the bed surface particles. Considering the impulse criterion, these motions are indicative of an energetic (the steeper the ascent, the

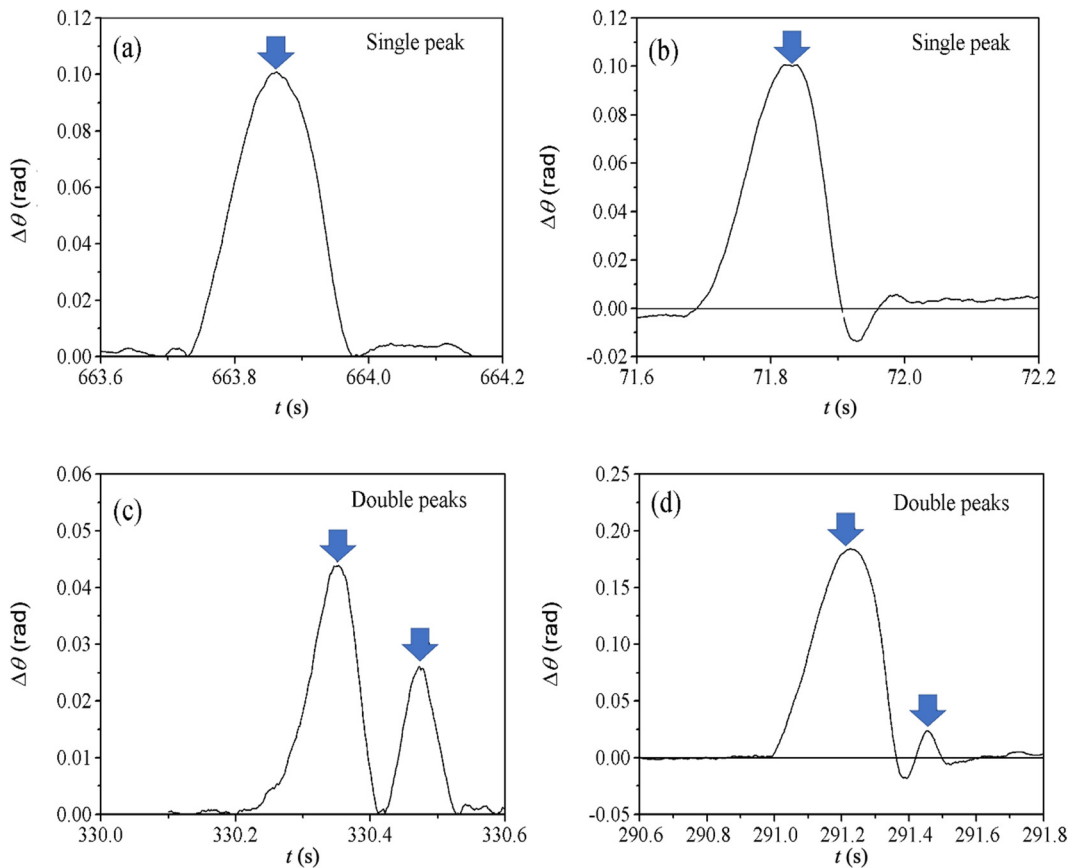


FIG. 4. Time series of exposed particle's angular displacements ($\Delta\theta$) demonstrating a range of typically observed (single to multi-peaked) rocking motions (a)–(f), until full displacement (g) and (h) is achieved. The down looking arrows denote the displacement peaks in the downwind direction. The vertical dotted lines in subplots (g) and (h) denote the moment when full particle entrainment is achieved.

Downloaded from http://pubs.aip.org/aip/pof/article-pdf/doi/10.1063/5.0047604/13831581/075117_1_online.pdf

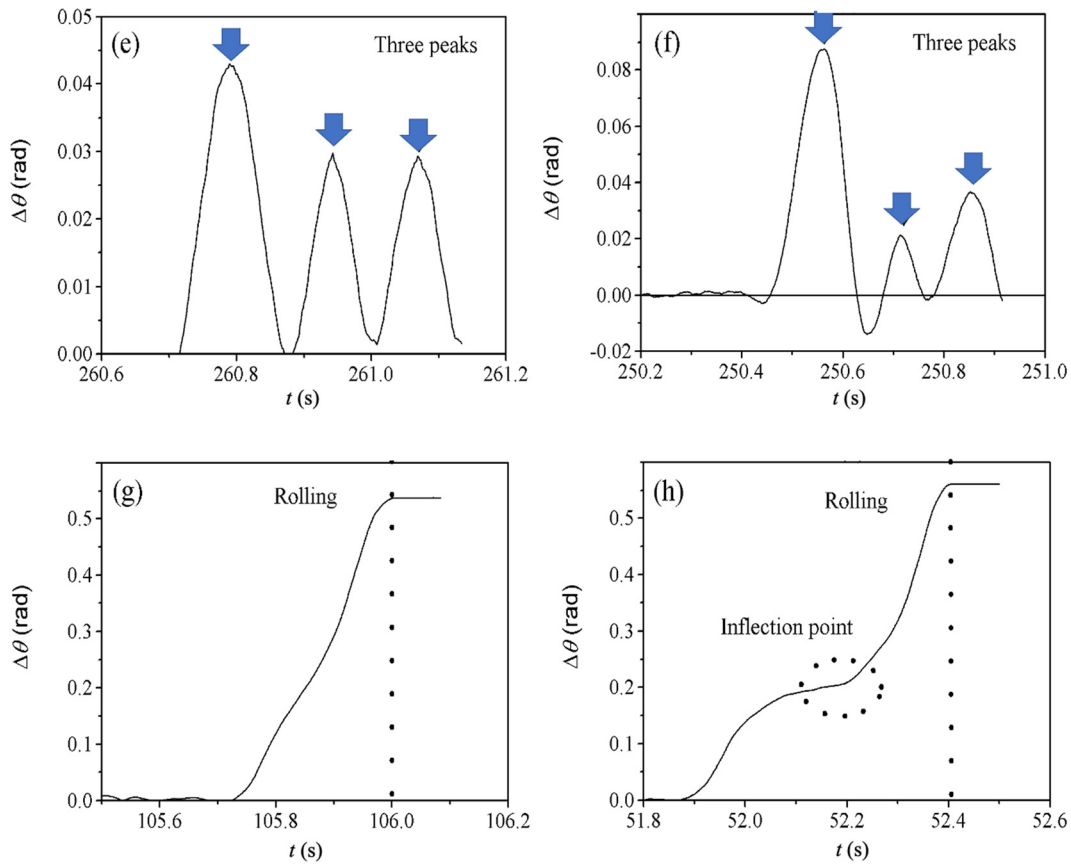


FIG. 4. (Continued.)

higher the flow energy), but yet short-lived flow structure (e.g., energetic but nearly instantaneous wind gust). The multiple-peak rocking events have two [Figs. 4(c) and 4(d)] or more [Figs. 4(e) and 4(f)] ascent–descent cycles demonstrative of a longer flow structures (greater length-scale) than before but not yet sufficiently energetic to fully dislodge the test particle, airflow structures advected over the test particle. Following the aforementioned classification for all the identified entrainment events, it is seen that the single-peak type events dominate the incomplete motion events, accounting for 86.8% of the sample of incomplete rocking motions. Even if these cases are occurring intermittently (Sherman *et al.*, 2019), it is highly probable that the occurrence of a sequence of rocking events may relate to the formation, evolution, and breakup of turbulent flow structures advected along the roughened bed surface. As eddies of sufficient size [trailing eddies as suggested by Valyrakis *et al.* (2010a) for water flows] are advected over the test particle, they may induce a corresponding response leading to one or more partial entrainments. The temporal distance of these entrainments will relate to the length-scale of these events and their advection velocity, which can help us to infer useful information for the flow field.

Likewise, the full incipient rolling is found to have two types based on the obtained displacement signals. These can be characterized by the duration that takes for the particle to be entrained, from

the instance of incipient entrainment to the peak of entrainment, into short, long, and very long rolling entrainments (Valyrakis *et al.*, 2010a, 2013). The dominated type (16/19), which may also be termed as “prompt dislodgement” according to Shih and Diplas (2014), is characterized by monotonically increased angular displacements, as shown in Fig. 4(g). The particle completes such dislodgements within 0.335 s on average. The increasing slope of displacement indicates sustaining acceleration over this dislodgement and implies that the temporal aerodynamic force always exceeds the resistance level in the dislodgement.

The second type of incipient rolling is typically characterized by an inflection point in its displacement signal, as shown in Fig. 4(h) (see dotted circle). The particle completes such dislodgements within 0.456 s on average, which is longer compared to the first type. At that instance [as marked by the dotted circle Fig. 4(h)], the particle decelerates to nearly zero upwind speed, resulting from a temporal imbalance of the resistance forces exceeding the instantaneous aerodynamic forces locally applied on the sphere. However, the deceleration phase is eventually interrupted (as opposed to the case of incomplete displacements) by the subsequent airflow structure accelerating the particle downwind, toward full entrainment. Such a case of full entrainment as described herein is similar to the “long displacement events” (Valyrakis *et al.*, 2010a) or “tardy dislodgement” events

(Shih and Diplas, 2014), specified for incipient entrainment in turbulent water flows.

It is also of interest to consider the temporal separation of rocking and rolling events. The case where the rolling (full) entrainment event is preceded by a rocking (incomplete) entrainment event may be indicative of a sequence of impulses advected over the test particle, as shown for water (Valyrakis *et al.*, 2010a; Shih and Diplas, 2014). After a careful study of the particle displacement record for all experiments, it is found that even though nearly all of the incipient rolling events (18/19) appear after rocking motions, their temporal separation is quite significant to associate one to the other, ranging from 0.3 to 40.047 s, with only 5.25% (1/19) of the intervals being at 0.3 s (all others are above 0.5 s). Figure 5 shows the case of minimum interval between a rocking and a rolling event (0.3 s). It can be seen that the rocking and incipient rolling are independent of each other, despite them being relatively close. Thus, it is expected that at near threshold flow conditions, rocking and rolling events are quite distinct and there is no interaction between them in the way they are defined, which allows for a robust classification of incipient entrainment events of coarse particles due to airflows.

As a response to turbulent aerodynamic forcing, the particle's displacement signal inherently contains a lot of rich information on the turbulence–particle dynamical interactions and turbulent airflow near bed structures. Similar to Valyrakis *et al.* (2010a) and (2013), but for water flows, the displacement event, specifically the downwind ascending phase, is driven by flow events, which consist of locally strong wind bursts lasting for a short duration. Then, the single-peak rocking containing individual ascending phases may be caused by a single flow event. The multiple-peak rocking containing several ascending phases may be dislodged by several discrete flow events. Likewise, the tardy incipient rolling as shown in Fig. 4(h) involving two-stage acceleration may imply that two separate flow events are involved in this event. These results are also similar to water flow induced transport due to a group of sweep events (Valyrakis *et al.*, 2010a). Nevertheless, because of the dominance of single-peak rocking and incipient rolling, with a sufficiently high temporal separation from other rocking events, the distinct flow event approach, as opposed to entrainment induced by a

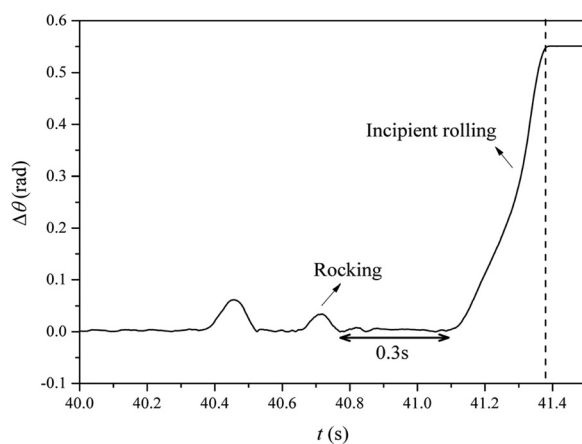


FIG. 5. Experimental demonstration of a series of rocking particle motions leading to complete rolling (full entrainment event). The vertical dashed line denotes the moment when full entrainment of the test particle is achieved.

sequence of flow events, is proposed to be the preferential mode for aerodynamic entrainment of coarse particles.

B. Stochastic assessment of particle entrainment

Due to aerodynamic flow turbulence, the entrainment of coarse solids under incipient conditions is a stochastic phenomenon. Herein, particle entrainment parameters, such as the angular displacement amplitude ($\Delta\theta_m$), the vertical amplitude (A_z), the ascending duration (t_a), and the interval time between rocking events (t_i), are probabilistically described, by attempting best statistical fits to the empirical distributions from the series of conducted experiments. It is found that the angular displacement amplitude $\Delta\theta_m$ follows the Lorentz distribution [Fig. 6(a)], while the vertical amplitude A_z and the ascending duration t_a both follow lognormal distributions [Figs. 6(b) and 6(c), respectively]. These probabilistic models are characterized by a left near-Gaussian part and a right long tail. The near-Gaussian part consists of relatively weak displacement events primarily from single-peak rocking, whereas the long tail is largely attributed to multi-peak rocking. The characteristics of the distributions of these parameters are instructive to gain a better understanding of the event-based turbulence-particle dynamics. Based on the conservation of energy, the increase in gravitational potential energy in the ascent phase (proportional to the vertical amplitude A_z) should be equal to the mechanical work done by the responsible flow event neglecting frictional losses [similar to the proposition of Valyrakis *et al.* (2013) for water flows]. Then, the mechanical work corresponding to the energy offered from sufficiently energetic flow events to particles should follow an identical probabilistic distribution with the vertical amplitude. Further, the energy of flow events is physically linked to the inverse of the ascending duration; highly energetic events will entrain the particle faster than lower energy flow events.

For near incipient aerodynamic flow conditions, rocking motions intermittently occur. The target particle remained immobile, resting on the bed surface for virtually the whole duration of the experiment, and displacement events occurred sporadically over a very short period (order of tens of milliseconds). Therefore, the interval time t_i follows a negative exponential heavy tailed-distribution, as shown in Fig. 6(d). Considering that rocking events are induced by bursting-like airflow events that are insufficiently energetic to dislodge the sphere completely, it is physically well justified that the interval time between rocking events t_i is found to follow a similar heavy tailed distribution with the interval between consecutive turbulent bursts (Sechet and Le Guennec, 1999; Valyrakis *et al.*, 2011a, 2011b).

C. Dependence of rocking motions on time-averaged wind speed

The particle's rocking frequency (f_r) is defined as the number of rocking events per unit time. Figure 7(a) reveals that the rocking frequency f_r rapidly increases with the time-averaged wind speed U . For example, the frequency at $U = 7.5$ m/s is about 1/50 of the value at $U = 8.2$ m/s. Early observations on 0.59–0.84 mm sand grains and 6.1 mm tapioca spheres report a rocking frequency of about 1.8 Hz (Lyles and Krauss, 1971), whereas the maximum frequency for 40 mm spheres used in this study is only 0.23 Hz, implying that larger and lighter particles have more distinct and well-defined response. The

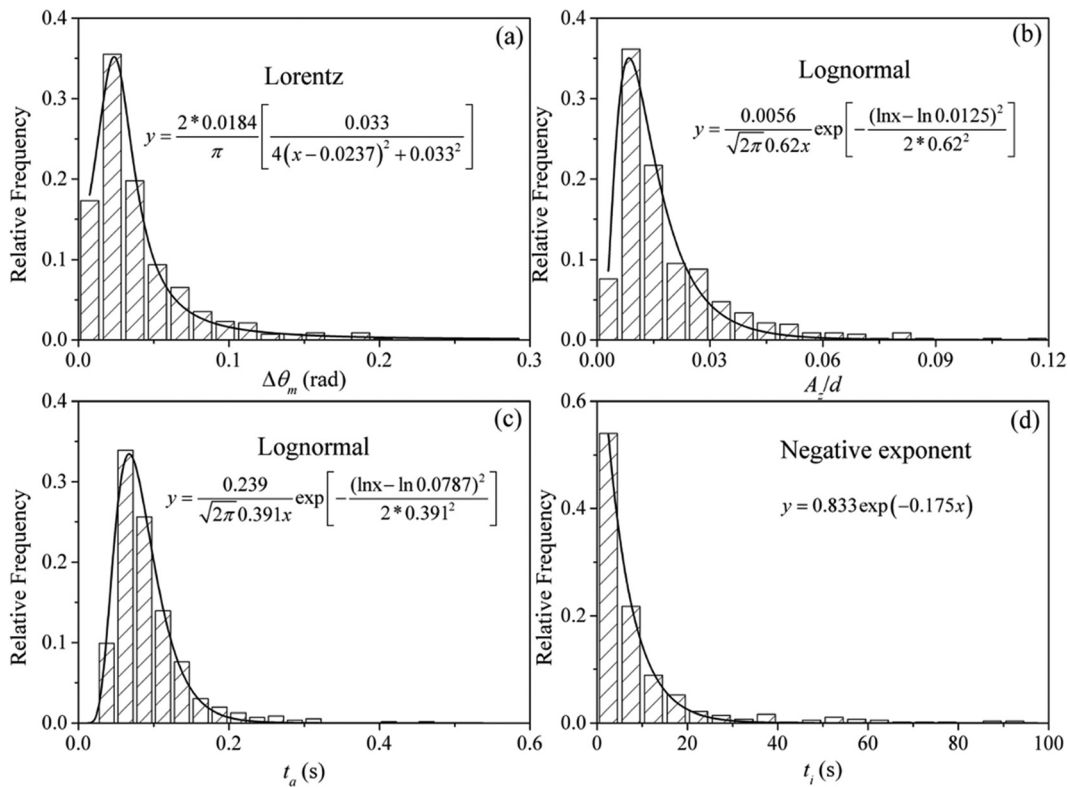


FIG. 6. Indicative probability distributions of particle motion characteristics: (a) magnitude of angular displacement, $\Delta\theta_m$, (b) vertical amplitude A_z , (c) duration of ascending motion t_a , and (d) interval between motions t_i .

good correlation between f_r and U suggests that it is possible to estimate the rocking frequency by means of time-averaged wind speed.

The average angular displacement amplitude ($\Delta\theta_m$) and ascending duration (\bar{t}_a) increase with the time-averaged freestream wind speed (U) until the level of 7.9 m/s, beyond which rolling motions start being more prevalent, as revealed by the decrease in \bar{t}_a and $\Delta\theta_m$,

shown in Figs. 7(b) and 7(c), respectively. This result is consistent with the observation of Williams *et al.* (1994) on relatively fine solid particles; once the wind speed exceeds the rolling threshold, strengthened airflow is conducive to rolling motion rather than rocking. This may be explained by the reduced amplitude and velocity of particle motion as it rolls downwind, while the flow energy is not sufficient to sustain

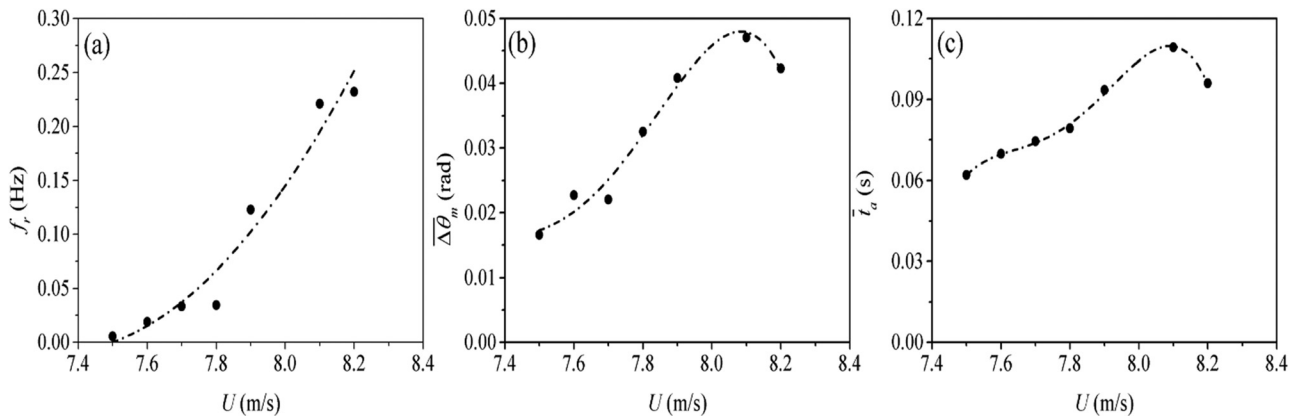


FIG. 7. Demonstration of the variation between the mean freestream wind speed U and (a) particle's rocking frequency, f_r , (b) mean magnitude of particle's angular displacement, $\Delta\theta_m$, and (c) average duration of ascending motions, \bar{t}_a .

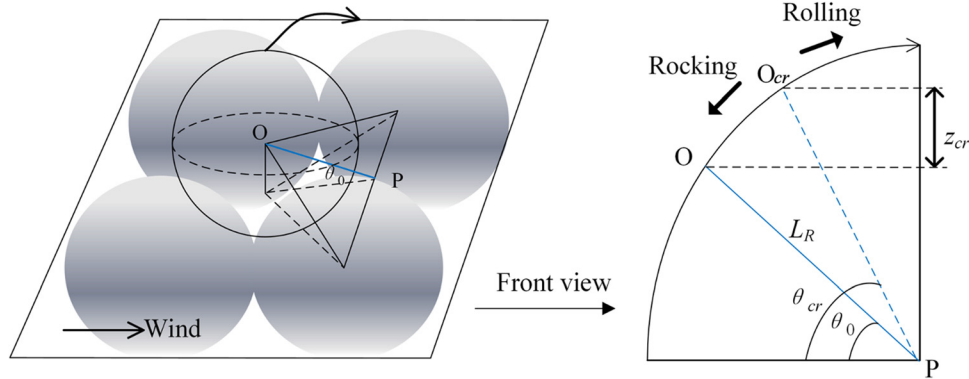


FIG. 8. (a) Schematic of the particle's pocket geometry, with focus on illustrating the plane of motion from a resting position (θ_0) to the threshold angular position (θ_{cr}) from where the particle can be entrained with just the influence of the mean wind speed, and (b) the plane of rotation and relevant geometrical characteristics are defined in the right figure. Also shown is the threshold vertical displacement (z_{cr}), distinguishing incipient rolling (full entrainment) from rocking (incomplete entrainment). L_R is the length of the lever arm (OP), defining the rolling of the center of the rolling particle around the axis of rotation P , defined by the line going through the center of the two downwind spheres around which the particle is rolling.

its motion (thus, the average \bar{t}_a and $\overline{\Delta\theta_m}$ are found to be decreased, compared to the case where rocking motions or a single entrainment, e.g., for lower wind speeds, is observed).

D. Transition from rocking to incipient rolling motions

In this section, the results of rocking and the transition to rolling are discussed in more depth. To this goal, a conceptual description of the dynamics of particle entrainment is offered, as is facilitated by the demonstration of Fig. 8. For a particle to fully roll out its pocket, it theoretically needs to reach the position where it is dynamically unstable (beyond which the slightest motion or push would allow for it to complete its entrainment downwind). In the case of no wind speed, this position is the peak of the saddle of the two base particles around which the particle is rolling. For the case of a finite mean downwind speed, the particle only needs to be lifted from its resting location (O in Fig. 8) to the new dynamically unstable location (O_{cr}) from where the particle will move downwind. This location will be reached earlier, given that the mean wind speed exerts a mean aerodynamic force, and the component of which (along the axis of particle's motion) will be enough to balance the force resisting the particle's motion (the particle's weight component along the axis of particle's motion).

It is interesting to observe the range of maximum angular displacements characterizing the particle's rocking motions. In this experimental study, the threshold level of angular displacements required to achieve full rolling entrainment, θ_{cr} , is measured to be 0.41π , as shown in Fig. 9. The distinct absence of rocking events (incomplete entrainments) for the range of $0.41\pi-0.5\pi$ is indicative that if a particle gets lifted up at or slightly beyond the threshold angular displacement position $\theta_{cr} = 0.41\pi$, it is highly likely that full entrainment by rolling will happen. This implies that θ_{cr} refers to a dynamically unstable position (O_{cr} in Fig. 8), where the increased mean flow aerodynamic forcing (due to the particle's greater exposure compared to the resting location, O in Fig. 8) is exactly balanced by a reduced resistance level. Any flow forcing beyond the mean forcing may be enough to dislodge the particle completely (similar to Valyrakis et al., 2011a, 2011b, but for water flows). It is physically sound to consider that this threshold level

is dependent on the mean wind speed (as explained before, the mean aerodynamic force balancing the particle's weight component resisting the motion) but relatively invariant to the turbulent fluctuations or energetic flow events responsible for initially pushing the particle out of its resting position (which occur intermittently for near threshold conditions). Naturally, particle characteristics regulating its resistance (specifically its size, shape, and density) are also expected to influence the threshold level of angular displacements required to achieve full rolling entrainment, θ_{cr} .

The threshold displacement level (z_{cr}) required to achieve full rolling entrainment, separating rocking (incomplete entrainments) and rolling motions (complete entrainments), can be obtained from the pocket geometry, as shown in Fig. 8, while considering the experimentally defined value for $\theta_{cr} = 0.41\pi$ (as empirically found in Fig. 9),

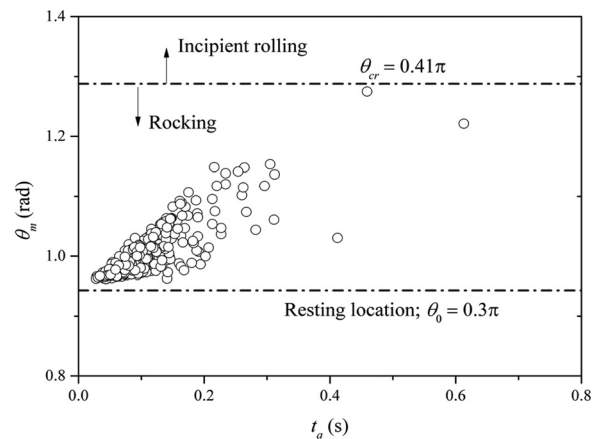


FIG. 9. Plot of peak angular positions for rocking particle motions against the ascending duration (t_a), helping to define the threshold level of angular displacements required to achieve full rolling entrainment, θ_{cr} , defined with the dash-dot horizontal line. Any displacements beyond this threshold, θ_{cr} , will result in full particle entrainment.

$$z_{cr} = L_R(\sin 0.41\pi - \sin \theta_0), \quad (1)$$

where θ_0 is the initial angular position of the exposed particle and L_R is the length of the lever arm (OP), defining the rolling of the center of the particle around the axis of rotation P . Parameters θ_0 and L_R depend on the pocket arrangement, meaning that Eq. (1) can be directly used for uniform well packed bed surfaces once the bed surface geometry (packing density and particle size) is determined. Past studies generally considered z_{cr} as the vertical distance from the resting positions to the highest location defined by the saddle of the downstream particles (e.g., Diplas *et al.*, 2008; Valyrakis *et al.*, 2010b; Lee *et al.*, 2012): $z_{cr} = L_R(\sin 0.5\pi - \sin \theta_0)$. Such a definition neglects the action of mean aerodynamic flow forcing in pushing the particle downwind after an initial rocking or rolling motion induced by an energetic flow structure, thus resulting in an overestimation of z_{cr} . Thus, this study is the first to experimentally derive an exact expression for the threshold displacement level (z_{cr}) required to achieve full rolling entrainment.

From an energy standpoint, Eq. (1) defines the minimum mechanical work (W_{cr}) required for airflow events to dislodge particles completely, which can be expressed as follows:

$$W_{cr} = F_g L_g (\sin 0.41\pi - \sin \theta_0), \quad (2)$$

where F_g is the particle's effective gravitational force (weight). This expression is vital to establish an appropriate energy criterion for the aerodynamic entrainment of coarse particles by rolling (similar to Valyrakis *et al.*, 2013) and can be used for predictive purposes to assess the probability of scour (Valyrakis *et al.*, 2011b, 2015) by turbulent eolian flows.

IV. CONCLUSIONS

This study is the first to experimentally measure the threshold displacement level for solid particles required to achieve their full entrainment by rolling on aerodynamically roughened bed surfaces. The results presented here, which constitute only statistics of the raw data, show the following points:

- (1) The rocking motion (incomplete entrainment) can be categorized into two types according to the number of downwind peaks in the displacement signal: single-peak and multi-peak rocking. Likewise, incipient rolling (full entrainment) can be distinguished into fast and tardy incipient rolling. Each motion type as well as its diverse characteristics can be thought off as signature responses corresponding to particular coherent flow event patterns. Single-peak rocking and fast incipient rolling represent the vast majority of incomplete and full entrainment events, suggesting that at near incipient flow conditions the flow structures that are sufficiently energetic to aerodynamically entrain coarse particles are temporally separated (rather than a sequence of burst-sweep events) and sporadically occurred.
- (2) The rocking parameters, including angular displacement amplitude, ascending duration, and interval time, can be probabilistically modeled with the Lorentz, lognormal and negative exponential distributions, respectively.
- (3) The transition from rocking to rolling is determined by a threshold angular displacement position, characterized by the mean flow and particle and bed arrangement properties. This value, experimentally found to be 0.41π for this study, is useful

in estimating more accurately threshold vertical displacements, for theoretical and predictive models that deploy relevant energy and impulse based criterion for the aerodynamic entrainment of coarse particles.

ACKNOWLEDGMENTS

This research was supported by the National Natural Science Foundation of China (Nos. 41171005 and 41071005) and the Ministry of Science and Technology of the People's Republic of China (No. 2013CB956000). The authors received valuable support from Lin G. M. for the measuring techniques. On behalf of all authors, the corresponding author states that there is no conflict of interest.

DATA AVAILABILITY

The data that support the findings of this study are available from the corresponding author upon reasonable request.

REFERENCES

- Anderson, R. S., Sørensen, M., and Willetts, B. B., "A review of recent progress in our understanding of aeolian sediment transport," *Acta Mech.* **1**, 1–19 (1991).
- Bagnold, R. A., *The Physics of Blown Sand and Desert Dunes* (Methuen, New York, NY, 1941).
- Batt, R. G., and Peabody, S. A., "Threshold friction velocities for large pebble gravel beds," *J. Geophys. Res.* **104**, 24274–24279, <https://doi.org/10.1029/1999jd900484> (1999).
- Bisal, F., and Nielsen, K. F., "Movement of soil particles in saltation," *Can. J. Soil Sci.* **42**, 81–86 (1962).
- Celik, A. O., Diplas, P., Dancy, C. L., and Valyrakis, M., "Impulse and particle dislodgement under turbulent flow conditions," *Phys. Fluids* **22**, 046601 (2010).
- Diplas, P., Dancy, C. L., Celik, A. O., Valyrakis, M., Greer, K., and Akar, T., "The role of impulse on the initiation of particle movement under turbulent flow conditions," *Science* **322**, 717–720 (2008).
- Diplas, P., Celik, A. O., Dancy, C. L., and Valyrakis, M., "Nonintrusive method for detecting particle movement characteristics near threshold flow conditions," *J. Irrig. Drain. Eng.* **136**(11), 774–780 (2010a).
- Diplas, P., Celik, A. O., Valyrakis, M., and Dancy, C. L., "Some thoughts on measurements of marginal bedload transport rates based on experience from laboratory flume experiments," *US Geol. Surv. Sci. Invest. Rep.* **5091**, 130 (2010b).
- Dwivedi, A., Melville, B. W., Shamseldin, A. Y., and Guha, T. K., "Flow structures and hydrodynamic force during sediment entrainment," *Water Resour. Res.* **47**, W01509, <https://doi.org/10.1029/2010wr009089> (2011).
- Giménez-Curto, L. A., and Corniero, M. A., "Entrainment threshold of cohesionless sediment grains under steady flow of air and water," *Sedimentology* **56**, 493–509 (2009).
- Greeley, R., and Marshall, J. R., "Transport of Venusian rolling 'stones' by wind?," *Nature* **313**, 771–773 (1985).
- Jia, S., and Wang, Z., "Simulation of aerodynamic entrainment with interparticle cohesions based on discrete element method," *Earth Surf. Processes Landforms* **46**, 1410–1418 (2021).
- Lee, H., Ha, M. Y., and Balachandar, S., "Work-based criterion for particle motion and implication for turbulent bed-load transport," *Phys. Fluids* **24**, 116604 (2012).
- Liu, Y., Jiang, X., Lee, C., and Hu, H., "An experimental study on the spatiotemporal evolution of sand waves/ripples in turbulent boundary layer airflow," *Phys. Fluids* **32**, 063304 (2020).
- Lyles, L., and Krauss, R. K., "Threshold velocities and initial particle motion as influenced by air turbulence," *Trans. ASAE* **14**, 563–566 (1971).
- Lyles, L., "Wind erosion: Processes and effect on soil productivity," *Trans. ASAE* **20**, 880–884 (1977).

- Molerus, O., and Burschka, A., "Pneumatic transport of coarse-grained materials," *Chem. Eng. Process.* **34**, 173–184 (1995).
- Molerus, O., "Overview: Pneumatic transport of solids," *Powder Technol.* **88**, 309–321 (1996).
- Nickling, W. G., "The initiation of particle movement by wind," *Sedimentology* **35**, 499–511 (1988).
- Pächt, T., Valyrakis, M., Zhao, X. H., and Li, Z. S., "The critical role of the boundary layer thickness for the initiation of aeolian sediment transport," *Geosciences* **8**(9), 314 (2018).
- Pächt, T., Clark, A., Valyrakis, M., and Duran, O., "The physics of sediment transport initiation, cessation and entrainment across aeolian and fluvial environments," *Rev. Geophys.* **58**(1), 1–58, <https://doi.org/10.1029/2019RG000679> (2020).
- Pächt, T., and Duran, O., "Unification of aeolian and fluvial sediment transport rate from granular physics," *Phys. Rev. Lett.* **124**, 168001 (2020).
- Sechet, P., and Le Guennec, B., "The role of near wall turbulent structures on sediment transport," *Water Res.* **33**, 3646–3656 (1999).
- Sherman, D. J., Li, B., Ellis, J. T., and Swann, C., "Intermittent aeolian saltation: A protocol for quantification," *Geogr. Rev.* **108**(2), 296–314 (2018).
- Sherman, D. J., Zhang, P., Martin, R. L., Ellis, J. T., Kok, J. F., Farrell, E. J., and Li, B., "Aeolian ripple migration and associated creep transport rates," *Geosciences* **9**, 389 (2019).
- Shi, P. J., Yan, P., Yuan, Y., and Nearing, M. A., "Wind erosion research in China: Past, present and future," *Prog. Phys. Geogr.* **28**, 366–386 (2004).
- Shih, W., and Diplas, P., "A micromechanical modelling approach for predicting particle dislodgement," paper presented at a symposium Sediment Dynamics from Summit to Sea, New Orleans, Louisiana, USA, 2014.
- Skidmore, E. L., "Soil erosion by wind: An overview," in *Physics of Desertification*, edited by F. El-Baz, and M. H. A. Hassan (Springer, Netherlands, 1986), pp. 261–273.
- Valyrakis, M., Diplas, P., Dancey, C. L., and Celik, A. O., "Incipient rolling of coarse particles in water flows: A dynamical perspective," in *River Flow 2010: Proceedings of the International Conference on Fluvial Hydraulics, Braunschweig, Germany, 08–10 September (2010a)*.
- Valyrakis, M., Diplas, P., Dancey, C. L., Greer, K., and Celik, A. O., "Role of instantaneous force magnitude and duration on particle entrainment," *J. Geophys. Res.* **115**, F02006, <https://doi.org/10.1029/2008JF001247> (2010b).
- Valyrakis, M., Diplas, P., and Dancey, C. L., "Entrainment of coarse grains in turbulent flows: An extreme value theory approach," *Water Resour. Res.* **47**, W09512, <https://doi.org/10.1029/2010WR010236> (2011a).
- Valyrakis, M., Diplas, P., and Dancey, C. L., "Prediction of coarse particle movement with adaptive neuro-fuzzy inference systems," *Hydrol. Processes* **25**(22), 3513–3524 (2011b).
- Valyrakis, M., Diplas, P., and Dancey, C. L., "Entrainment of coarse particles in turbulent flows: An energy approach," *J. Geophys. Res.* **118**, 42–53, <https://doi.org/10.1029/2012JF002354> (2013).
- Valyrakis, M., Michalis, P., and Zhang, H., "A new system for bridge scour monitoring and prediction," in *Proceedings of the 36th IAHR World Congress (2015)*.
- Zhang, P., Sherman, D. J., and Li, B., "Aeolian creep transport: A review," *Aeolian Res.* **51**, 100711 (2021a).
- Zhang, S., Nielsen, P., Perrochet, P., and Jia, Y., "Multiscale superposition and decomposition of field-measured suspended sediment concentrations: Implications for extending 1DV models to coastal oceans with advected fine sediments," *J. Geophys. Res.* **126**, e2020JC016474, <https://doi.org/10.1029/2020JC016474> (2021b).
- Wang, P., Zhang, J., Dun, H., Herrmann, H. J., and Huang, N., "Aeolian creep transport: Theory and experiment," *Geophys. Res. Lett.* **47**, e2020GL088644, <https://doi.org/10.1029/2020GL088644> (2020).
- Williams, J. J., Butterfield, G. R., and Clark, D. G., "Aerodynamic entrainment threshold: Effects of boundary layer flow conditions," *Sedimentology* **41**, 309–328 (1994).